Integrated interferometers as a new platform for low cost gas chromatography detection

Pomme Hirschauer, Benoît Paris, Sonia Messaoudene, Maryse Fournier, Bertrand Bourlon, Yanxia Hou, Florence Ricoul, Loïc Laplatine

Integrated interferometers as a new platform for low cost gas chromatography detection

Authors

Pomme HIRSCHAUER*
Benoît PARIS*
Sonia MESSAOUDENE*
Maryse FOURNIER*
Bertrand BOURLON*
Yanxia HOU+
Florence RICOUL*
Loïc LAPLATINE* (loic.laplatine@cea.fr, 17 avenue des Martyrs, 38000 Grenoble, France)
* Univ. Grenoble Alpes, CEA-LETI, 38054 Grenoble cedex, France
+ Univ. Grenoble Alpes, CEA, CNRS, Grenoble INP, IRIG, SyMMES, 38000 Grenoble, France

Abstract

Gas chromatography is a reference method for gas analysis. As part of efforts to miniaturize gas chromatography systems, the miniaturization of detectors is essential. In this work, we report a new integrated photonic platform for gas chromatography analyte detection. The fabricated silicon die integrates Mach-Zehnder interferometers into low dead volume microfluidic channels, with coherent cost-effective detection scheme with a fixed 850 nm wavelength laser. A proof of concept is demonstrated with the separation and detection of three volatile organic compounds: heptane, octane, and toluene. Peaks' widths at half height range from 1 to 5 seconds. Peaks are very well resolved by our system, which acquires more than 100 points per second. From a heptane dilution range, we evaluate the limit of detection of our system to be the headspace of a 0.22% heptane concentration solution. To our knowledge, these are the first integrated Mach-Zehnder interferometers reported for gas chromatography detection. This work could open new strategies for fast low cost and low limit of detection specific gas chromatography silicon micro-detectors.

Keywords

Integrated photonics; Mach Zehnder interferometer (MZI); Gas chromatography (GC);

Volatile organic compound; Gas sensor

Introduction

Volatile organic compounds (VOCs) are organic molecules with high vapor pressure. Their detection, quantification and identification are increasingly demanded in various fields including food quality control [1], [2], industry [3], [4], medical diagnosis [5], [6], and air and water quality monitoring [7], [8].

A standard and quantitative technique to detect and identify VOCs is gas chromatography (GC) coupled to mass spectrometry (MS). GC separates compounds of a mixture based on their differential affinity with a chemical lined into a capillary tube, through which the gas mix travels. MS successively detects and identifies each compound as it gets out of the tube. This approach is very precise and reliable. However, the main limitation is that GC-MS is a bulky, costly and complex laboratory system, which requires skilled operators.

Since the first work of Terry et al in 1979 [9], scientists have been trying to tackle the issue of on-site complex gas analysis by miniaturizing gas chromatography and coupling it to detectors less bulky than mass spectrometry ([10], [11], [12], [13]). Gas chromatography systems perform three main functions: sample injection, sample separation and sample detection. Detector miniaturization was made available by the advent of micromachining techniques and progress in Complementary Metal Oxide Semiconductor (CMOS) fabrication

processes. Main approaches in the literature include electronic transduction detectors, ionization detectors, gravimetric detectors, thermal conductivity detectors, and optical transduction detectors.

Electronic transduction micro-detectors are based on the modification of the capacitance ([14]) or resistance ([15], [16], [17], [18]) of the micro-detectors upon absorption or adsorption of VOCs.
Thermal conductivity detectors (TCDs) are based on the measurement of a change in gas thermal conductivity, which induces a change of temperature of a resistor, which in turn affects its recorded resistivity ([19], [12], [13]).
Ionization micro-detectors rely on modification of an electric current upon ionization of VOCs by a helium flame (Flame Ionization Detector, FID) or a photon beam (Photo Ionization detector, PID). FIDs require a helium flow, which prevents its portability. PIDs, on the other end, often require calibrations on target analytes, and cannot detect high ionization energy compounds. Both these detectors are destructive.
Gravimetric micro-detectors mechanically oscillate at a frequency that depends on their mass ([20], [21], [22], [23]). Absorption of VOCs in a polymer film covering the oscillating part ([20]), or direct adsorption of VOCs on the oscillator surface ([21], [22], [23]) modifies the sensor's mass and shifts its resonance. However, the electronics needed to drive and control these micro-detectors are complex, involving current sources fast enough to respond to the resonant frequency of the oscillators, and precise spectrometers to monitor frequency changes.

We are interested in another type of miniaturized GC micro-detectors: integrated photonics sensors, based on the ability to guide light through materials with a high refractive index. Integrated photonic circuits offer three main advantages. Firstly, their fabrication is based on the CMOS industry, making them cost-effective for high-volume production. Secondly, they have a low footprint, making it possible to include many different components on small silicon dies. Finally, tailoring of circuits enables a myriad of optical operations.

Most refractive index sensing integrated photonic detectors involve measuring an optical spectrum shift upon VOCs adsorption. It is the case for Fabry-Pérot detectors ([24], [25]), photonic crystals [26], and micro-ring resonators [27], [28], [29]. Acquiring optical spectra takes a non-negligible amount of time, which limits acquisition rate and thus time resolution of chromatograms. It also requires the use of an accordable source, which increases the system cost compared to a single frequency source. On top of that, ring resonator and photonic crystal fabrication face challenges due to necessity of structures with very small dimension.

Mach-Zehnder interferometers (MZIs) are integrated photonic structures that do not need to be as small as ring resonators and photonic crystals. They are composed of two waveguides, whose geometrical properties and environment may differ. When an external stimulus alters the properties of one of the waveguides respective to the other, it modifies the phase difference between the two arms, which influences the interference pattern created upon recombination of light from both arms.

This principle has been widely exploited by the sensor community. In the 1990s, pressure sensors were designed with an arm located on a membrane sensitive to mechanical strain ([30], [31]). Nowadays, MZIs are widely used for the development of biosensors. The change in the refractive index of an antigen-grafted sensing waveguide enables antibody/antigen interaction monitoring for immunosensors ([32], [33], [34]). The same principle was used to monitor *in vitro* biochemical reactions ([35]), or to detect target contaminant in water or biological fluids ([36]). The literature also offers examples of MZI detectors for VOC detection in gas phase.

In most examples, the sensing arm is coated with a material chosen either to improve its sensitivity to VOCs or to tailor the selectivity of the sensor. Coating the MZI sensing arm with porous materials or polymers improves the MZI sensitivity by providing more adsorption sites for VOCs ([37], [38], [39]). In addition, absorption of VOCs into the polymer may cause its swelling, thus further affecting its bulk refractive index ([38], [39], [40]). The disadvantages of this approach is that it slows down the sensor response by imposing compounds' diffusion delays.

The bio-functionalization of a detector matrix, in order to adapt detector selectivity, has also been studied in the literature. For example, bio-functionalization with peptides enables compounds to be identified by recognition of their interaction pattern on the bio-functionalized matrix ([41], [42]).

In this study, we propose, for the first time, to use MZIs as gas chromatography micro-detectors. As soon as the sample arrives on the die, the VOCs adsorb onto all available surfaces, including the bare sensing waveguide surface. This increases the waveguide's effective index by interacting with the guided mode's evanescent field. The change in effective index modifies the phase delay φ between two arms of the MZI. A coherent detection scheme translates the phase shift evolution of one MZI into the relative evolution of its three outputs' intensity evolutions. The coherent detection presented here does not require accordable wavelength operation or optical spectrum acquisition to operate, and has a constant sensitivity whatever the phase difference ([43]). We have packaged the photonic die to meet both GC and optical operation requirements. We have demonstrated the performance of this portable GC detector for the detection of three analytes with a heptane detection limit close to 0.22 % vol/vol. This is a promising result for future on-site rapid and cost-efficient portable GC.

Experimental section

Die fabrication and packaging

Details on die design and fabrication can be found in ref [41].

Most mature integrated photonic platforms rely on Si to guide light and perform optical operations with low losses. We have chosen to work at λ = 850 nm to enable light detection possible by CMOS imagers, paving the way towards cost-efficient microsystems. At this wavelength, Si is not transparent. Si_3N_4 was therefore used as a guiding material, thanks to its transparency in the visible and near infrared range. Its lower index contrast with respect to SiO_2 makes it less sensitive to waveguide roughness and therefore suffers fewer propagation losses : $n(SiO_2) = 1.45, n(Si) = 3.5, n(Si_3N_4) = 2$. Another advantage of Si_3N_4 over Si is its lower thermo-optic coefficient, making it less sensitive to temperature fluctuations.

The fabrication at CEA-Leti's 200 mm cleanroom involves Si_3N_4 layer deposition and patterning on thermally oxidized Si substrates, cladding of the whole die with SiO_2, and opening of windows on top of MZI sensing waveguides by dry and wet etching, as represented in figure 1.

Before packaging, dies were rinsed with isopropanol, immersed in acetone for one minute, then immersed again in an isopropanol bath for another minute.

Microfluidic packaging of the photonic die was needed to preserve chromatographic peak separation by limiting dead volumes on flow path. The packaging consists of a 7.3 x 11.4 mm microfluidic lid composed of 1-mm-tall PMMA stuck to the photonic die by Nitto D5381B double-sided tape. We designed the microchannels of this lid assembly using Klayout and Inkscape, and laser-machined it using the Trotec Speedy 100 laser cuter, according to the pattern visible in figure 2. The microchannel was about 500-µm-deep, 10-mm-long, 5 mm of which are 500-µm-wide (for microchannel flow routing), and 5 mm of which are 1-mm-wide, over the MZIs' sensitive arms. Its dead volume is therefore of the order of 4 µL.

Once the photonic die and microfluidic lid are assembled, the die must be connected to the GC system. Deactivated fused silica capillary 160-2255 from Agilent Technologies were inserted on either side of the microchannel and glued using the Polytech UV 2195 glue.

Sample preparation

The samples used in this work are the headspaces of VOC solutions in mineral oil. The liquid VOC solutions were purchased from Sigma Aldrich, and have > 99 % of purity, with the exception of heptane, which has 98 % of purity, and o-xylene and benzene, which have 97 % of purity. The solvent is mineral oil M8410 from Sigma Aldrich. All products are stored at room temperature before use. Samples were prepared in our laboratory, in transparent glass vials capped with PTFE-lined solid screw caps, using graduated pipettes to adjust their relative volumes of mineral oil and VOC solute. For very low heptane concentration, we diluted a more concentrated heptane stock solution prepared for this purpose, of concentration identical to that of solution 11 presented in table 2. Before use, vials were left to stand at least one hour at 20°C and uncontrolled laboratory humidity was measured at 38% ± 2%.

The vials used for chromatographic proof of concept (figure 4) are the headspaces of 15 mL vials, in which 1 mL of solution has been prepared. Each solute is present at a concentration of 3% in the solutions filling the vials (30 µL solute and 970 µL mineral oil). One of the vials used for this experiment contains 3% of each of the three liquid VOCs (heptane, octane, and toluene): 30 µL of each and 910 µL of mineral oil.

The samples used to measure sensor sensitivity were prepared in 22 mL vials, containing 5 mL of solution. Concentrations ranged from no heptane at all to pure heptane.

We also used an Agilent 7890B GC system in which samples were injected as liquids with a split/splitless automatic liquid sampler (7693A). To prepare a benzene, toluene, ethylbenzene, and xylenes (BTEX) mixture sample, the same volume of each aromatic (benzene, toluene, ethylbenzene and o-xylene) were measured with graduated syringes and poured into a 2-mL glass vial, without any solvent.

Sampling and injection in analytical setup

The sample vials are connected to a sample selection device, which consists of the 8-port distribution valve V-D-1-8-050-C-P purchased from AMF, actuated through USB-sent Python commands. The fluidic connection is made by 1/16'' external diameter Z226955 green PEEK tubes, one side into the distribution valve, and the other glued to the vial caps in such a way that the end of the tube reaches inside the vial headspace. In fact, the vial caps are connected twice by a hole in their caps: a second PEEK tube is used to connect the vials to the 9-ports manifold P-191-01 purchased from Cluzeau Info Labo.

The single output port of the distribution valve is connected to the 2-position 6-ports injection valve DC6WE from Vici Valco. Only one vial is connected to the distribution valve's unique output at a time. The flow towards the injection valve is monitored by mass flow controller F-200DV from Bronkhorst. There are two ways of implementing sample flow to the injection valve. The first involves a pressure source upstream of the manifold. In this case, the flow controller is placed between the pressure source and the manifold input, and the distribution valve's output is connected directly to the injection valve. The second involves a vacuum source downstream of the injection valve. In this last case, the flow regulator is placed between the output of the distribution valve and the injection valve, while the manifold input port is left to laboratory ambient air.

The 2-position valve was analogically operated by an Arduino Uno card controlled by Python commands. Its six ports are connected to two flow paths and a sampling loop (stainless steel 5 µL sampling loop SL5CUW purchased from Vici Valco). The sampling loop can be placed either on the sample flow path to be loaded with the sample, or on the gas chromatographic flow path, to inject its contents into GC column.

The gas chromatographic flow is the mobile phase flow, the gas used to transport the sample through the GC column for separation. We use nitrogen of 99.9999% purity, supplied by Air Liquide. Its flow rate is controlled by a Bronkhorst mass flow controller upstream of the injection valve. The chromatographic separation column is an Agilent DB-5MS column, cut to 3 meters long. Its internal diameter is of 320 µm, and its stationary phase, the coating used to retain analytes inside, is non-polar. The end of the GC column is connected to one of the photonic die's packaging's capillary using the universal press-fit glass union 5190-6979 from Agilent.

Chromatographic injection consists of three main steps. First, baseline stabilization. During this step, the sampling loop is not on the flow path of the GC column. This allows sampling loop, GC column and photonic die purge. The second step is sample loading. During this step, the distribution valve allows the vial to pass through to the sampling loop. The third step is chromatographic injection, during which the sampling loop is placed on the gas chromatographic flow path to inject its contents to analysis device. The time reference t = 0 s for the chromatograms corresponds to the start of injection of the sampling loop contents.

The syringe of the split/splitless injector has a volume of 500 nL, the injection volume was set to 50 nL and the split ratio was set to 308 so that approximately 36 ng of each aromatic is injected towards the column. The injector is heated at a temperature of 250°C, which ensures that the solutions are fully vaporized before the column inlet. The GC flow rate is measured equal to 1 mL/min with helium as carrier gas. A 5-meter-long SLB-5MS GC column of internal diameter 250 µm and 0.25 µm stationary phase thickness from Supelco was used. The detection was performed in two stages: first, the GC column output was directed towards the MZI, then the output of the non-destructive MZI detector was brought to the FID (temperature 300 °C, airflow 400

mL/min, hydrogen flow 30 mL/min, no makeup gas). Separation was conducted at room temperature, with no use of the GC oven.

Optical detection setup

The photonic die was placed on an aluminum base. The light source and camera were placed upside down, around 1 mm above the die. The three-axis displacement stages on which they were mounted facilitate their alignment.

The light source is an 850 nm single-mode vertical-cavity surface-emitting laser (VCSEL) purchased from Lasermate. The die is optimized for TM polarization, which means that the MZI's Free Spectral Range (FSR) is higher for the TM mode than for the TE mode. For this reason, a polarization filter was placed between the VCSEL and the die input, so that only TM mode is guided in the die.

The optical detector is a 512-pixel resin-sealed linear CMOS imager S10227-10 purchased from Hamamatsu and read by a Coptonix USB Line Camera 8M PCB board. Images of the 48 outputs corresponding to the 16 MZIs are acquired at a frequency of 200 Hz.

We developed a real-time Python software to extract phase shift from the image of the three outputs of each MZI. In this work, we averaged the phase shifts from four identical MZIs to improve the signal to noise ratio.

The first processing step consists in an image segmentation to recover each of the three optical outputs from each MZI. Intensities $P_i(t)$ for i among {1, 2, 3} is expressed as:

$$P_i(t) \propto 1 + V.cos\left(\varphi(t) + (i-1) * \frac{2\pi}{3}\right) \qquad (1)$$

In this expression, V is the visibility of the interference pattern related to the length and the linear losses of the two arms of the interferometer, and φ the phase difference between the two recombined MZI arms.

The second processing step is raw phase evolution computation thanks to three outputs intensities' monitoring. Trigonometric operations on P_1, P_2 and P_3 expressions lead to express phase as $\varphi = \arg(x + iy)$, where:

$$\begin{cases} x = 2 * P_2(t) - P_1(t) - P_3(t) \\ y = \sqrt{3}(P_1(t) - P_3(t)) \end{cases}$$

The third step is a phase calibration, which aims to overcome possible phase miscalculations due to parameters affecting the phase calculation, such as fabrication and design imperfections, dust on the imager, on the die, or damaged grating couplers. The principle of this calibration is detailed in [44].

A phase unwrapping is necessary to witness for the continuity of the phase evolution even for phase shifts higher than 2π. The absolute phase φ(t) of each MZI has no particular interest and only the phase shift Δφ(t) is presented, with $\Delta\varphi(t) = \varphi(t) - \varphi(0)$.

Results and discussion

In this section, we first present the results of the photonic die design optimization. We then demonstrate successful detection of three VOCs in a VOC mix. Finally, we explore the response of the detector to a range of heptane concentrations.

Silicon photonic die design

Our design choices were motivated by a concern for the cost-effectiveness of portable detectors. It led us to choose Si_3N_4 waveguides at a working wavelength of λ = 850 nm, which enabled us to use both an inexpensive CMOS imager and a single-mode polarized VCSEL.

A single grating coupler couples light from the VCSEL into the silicon die waveguide. Multimode interferometers (MMI) split light equally into each of the photonic die's 16 MZIs, and then between both arms of each MZI. Another MMI (2 by 3) recombines and immediately divides light into three light paths dephased of 120°. Each output of this last MMI is directed to a grating coupler for imaging. The 48 output grating couplers

are aligned on die, so a linear detector can be used to monitor all of them simultaneously. The input and output grating couplers were optimized for a light incidence angle of 11.6° in air, the waveguides were optimized for TM polarized light at λ = 850 nm, and the MMIs were optimized to perform their function. The TM-polarization waveguides are designed as large as they can be while staying monomode, to minimize optical loss. This optimization leads to waveguides of width 760 nm. To reduce footprint, the MZI arms were folded into spirals, with the number of turns, the curvatures of the turns, and the spaces between adjacent turns optimized for a good trade-off between bendloss, crosstalk and footprint reduction.

Thanks to our optimization work, a 7.25-mm-large and 21.7-mm-long die hosts different interferometers matrices and test structures. The MZIs used in this work (see figure 1) have a footprint of 200 µm by 400 µm, and are repeated with a 575 µm horizontal pitch and a 450 µm vertical pitch. The matrix of 16 MZIs, organized in 4 rows of 4 MZIs, occupies 5 square millimeters. The die's input and output grating couplers, routing waveguides, and MMIs used to perform optical operations add an additional area of close to 10 square millimeters.

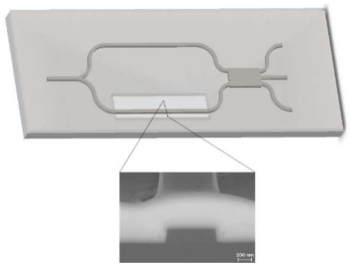

Figure 1. Schematic illustration of a coherent detection Mach-Zehnder interferometer with a cladding opening on one arm. Inset: SEM image of a sensing waveguide.

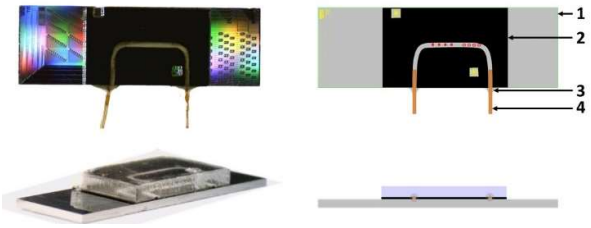

Figure 2. Left: photos of the packaged die, top view and perspective view. Right : schematics of the packaged photonic die, with : (1) photonic die with alignment patterns (yellow) and MZI sensing arms (red) - (2) micromachined fluidic lid (tape and PMMA) – (3) glue – (4) deactivated capillary. The die is 7.25-mm-large, 21.7-mm-long, and 0.7-mm-high.

Detection of GC analytes

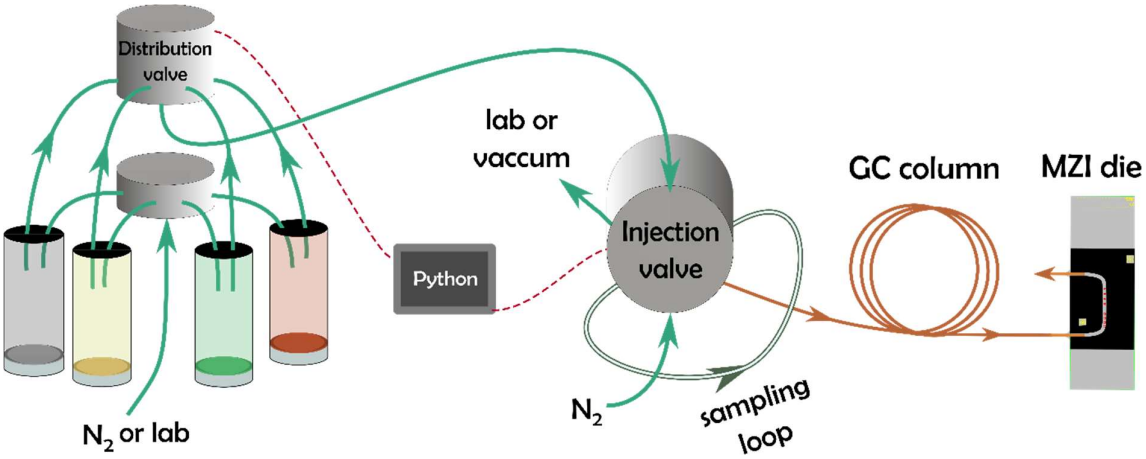

Figure 3. Gas flow schematics of the chromatographic setup.

We acquired consecutive chromatograms of four different VOC samples containing either a pure VOC in mineral oil (for three of them), or a mixture of VOC solutions in mineral oil (for one of them). For all four samples, the concentration of each VOC is 30 µL of compound for a total solution volume of 1000 µL. To obtain a chromatogram, 5 µL of the sample headspace is loaded in the sampling loop and injected at a mobile phase flow rate controlled at 1 mL/min. To load the sampling loop, a nitrogen source is plugged upstream of the sample vials to induce sample flow to the distribution valve (figure 3).

The four chromatograms showed on figure 4 present a peak at a retention time of around 15 seconds, with an amplitude of the order of 0.1 radians. This corresponds to the time required to purge the volume of the chromatographic column. This peak indicates the arrival of the mobile phase on the photonic die.

The first three chromatograms, corresponding to pure VOC samples, show an additional peak, with a height of around 0.12 radians. The peak parameters for each of these three VOC samples are gathered in table 1. All three pure VOC samples, of close VOC concentration, reached close phase levels at their peak. This indicates that the detector has the same order of magnitude sensitivity for heptane, toluene and octane.

The chromatogram of the mixed VOCs shows three distinct peaks at retention times, demonstrating a good separation of the three VOCs present in the mixture. This is the first observation of the use of integrated MZIs as a gas chromatographic detector. The peaks have a slightly asymmetrical Lorentzian shape, with the rising edge slightly longer than the falling edge. Both the peaks' full width at half maximum (FWHM) and the rising edge duration increase with retention time, indicating that the GC columns broadens peaks more when the compound is more retained.

It seems that heptane has a lower affinity than octane and toluene with the non-polar stationary phase of the GC column, since it leaves the GC column earlier. For all analytes, retention time when the analyte is pure and retention time when the analyte is in a mix bear only a 1% difference. The compound's retention times is slightly smaller when the compound competes with other compounds in the sample. Indeed, the VOC mixture's chromatogram peaks attain their maximum earlier because they reach a lower phase than when each VOC is injected alone (around 0.06 radians instead of 0.12 radians). This is due to the concurrent evaporation of heptane, toluene, and octane in the sample vial, which limits the quantity of each VOC that is actually injected into the GC column.

Table 1. Analysis of peaks present in chromatograms in figure 4.

VOC sample	Retention time	Height	FWHM	Rise duration
Heptane	$t_r = 82.4\ s$	0.13 rad	2.4 s	4.4 s

Toluene	$t_r = 144.8\ s$	0.12 rad	4.7s	6.8 s
Octane	$t_r = 206.7\ s$	0.12 rad	7.0 s	10.7 s
Heptane Toluene Octane	$t_r = 81.8\ s$ $t_r = 144.5\ s$ $t_r = 204.3\ s$	0.06 rad 0.08 rad 0.04 rad	2.3 s 4.5 s 7.1 s	3.7 s 6.4 s 8.3 s

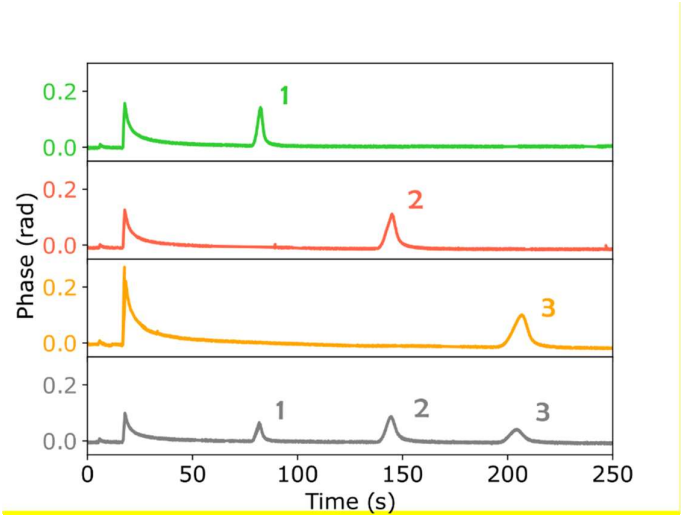

Figure 4. Chromatograms obtained for the injection of the headspace of solutions of (green) heptane, (red) toluene, (yellow) octane, and (grey) a mix of heptane, octane and toluene.

In figure 5, we compare the chromatograms obtained upon separation of a BTEX mixture on the commercial GC setup with our detector and with the FID. The MZI BTEX chromatogram was post-processed by fitting its fourth order polynomial baseline.

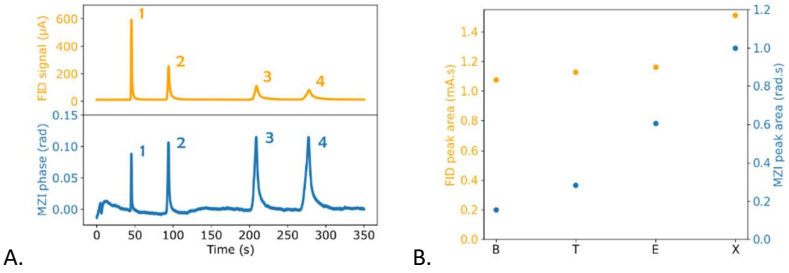

Figure 5. A : Compared chromatograms of a BTEX mix on the MZI detector (blue) and the FID detector (orange). Peaks are identified, from experience on Agilent GC system, as: 1-Benzene, 2-Toluene, 3-Ethylbenzene, 4-o-Xylene. B: Heptane peak areas on the MZI detector (blue) and the FID detector (orange).

Both chromatograms broadcast four peaks at consistent retention times. They differ by the evolution of peak shapes and their signal to noise ratio. On both detectors, peaks tend to broaden with increasing molecular weight. The peaks seem to have roughly the same height for all aromatics on the MZI phase signal, while the peak heights decrease with broadening on the FID signal. The right-hand side figure confirms that, indeed, the peak area is almost constant for FID chromatogram, while the peak area increases in MZI chromatogram. This trend indicates that the MZI signal is sensitive not only to injected mass of the compounds, but also to their adsorption and desorption affinities on the sensing waveguide. These affinities may depend on the compounds' size, molecular weight and molecule structure, as suggested in the literature [22].

Sensitivity characterization

We performed, on the home-made GC system presented Figure 3, consecutive chromatograms of 16 heptane solutions of different concentrations, ranging from pure heptane to no heptane sample, as presented in table 2. The samples were willingly chosen to span four orders of magnitude of concentration. This enables to compute the sensitivity of the detector at low concentrations.

Table 2. Heptane samples concentrations.

Solution	V_{C7} / V_{tot}
0	0 %
7	0.05 %
8	0.075 %
9	0.1 %
10	0.2 %
11	0.5 %
12	0.8 %
13	1 %
14	2.5 %
15	5 %
16	7.5 %
17	10 %
18	25 %
19	50 %
20	75 %
21	100 %

The flow rate of the mobile phase was monitored at 2 mL/min, and the solutions were injected starting with the most concentrated and working towards the least concentrated. Chromatograms of each sample were acquired twice. The first dataset was deprecated, since it was considered likely for the injection to be polluted by the previous sample's injection. The second chromatograms acquired for each sample are plotted in figure 6A. A peak about 3-radian-high is measured at a retention time of 8 seconds. This corresponds to the time needed to purge the volume of the chromatographic column. This peak points out the arrival of the mobile phase on the photonic die. This peak may be due to water being loaded in the system upon connection of mobile phase flow to sampling loop.

We focused on the chromatographic peak corresponding to heptane, which starts to arrive at a retention time of 34 seconds. We noted that concentration has an impact on the heptane peak in both height and width, making area the appropriate data to study in these results.

We baseline-fitted the tail of the 8 seconds peak to overcome the impact of the tail on the heptane peak area calculation. The processed data around the heptane peaks are presented in figure 6B. The most concentrated heptane peaks have a tendency to fronting, typical of GC column overload. This effect becomes less significant as heptane concentration decreases.

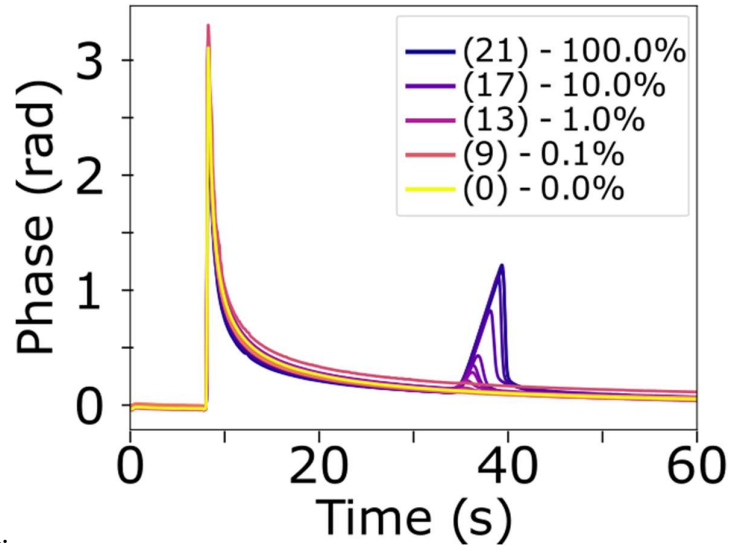
(21) - 100.0%
(17) - 10.0%
(13) - 1.0%
(9) - 0.1%
(0) - 0.0%
Phase (rad)
Time (s)

A.

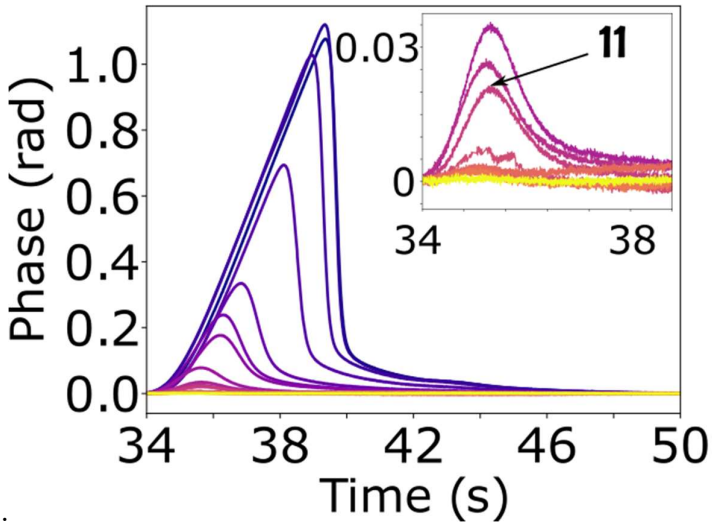
Phase (rad)
Time (s)
11

B.

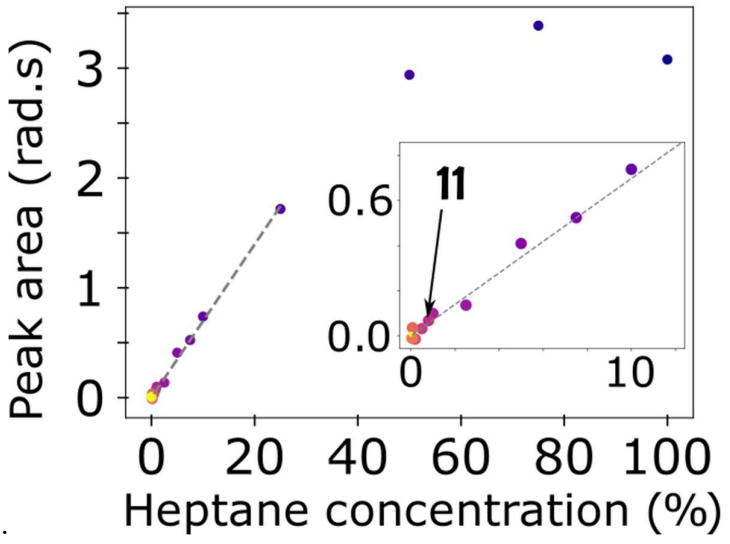
Peak area (rad.s)
Heptane concentration (%)
11

C.

Figure 6: A. Raw chromatograms. B. : post-processed chromatograms obtained for 16 heptane samples at different concentrations, the darkest purple being solution 21, the most concentrated sample. B inset: post-processed chromatograms for samples of heptane concentrations under 1%. C: heptane peak area evolution with heptane concentration. The dashed line is a linear fit. C inset: heptane peak area evolution for samples of concentrations under 10%. The arrows point at data from solution 11, of concentration of 0.5 % heptane, which is the last to be considered as detectable.

The processed data were integrated on the peak's width to compute the heptane peak area. Heptane peak area evolution upon heptane concentration in sample vials is plotted in figure 6C. At low concentrations, our detector is linear with respect to concentration. The linear regression on the data corresponding to the 13 samples of heptane concentration under 25% has a coefficient of determination of $R^2 = 0.996$, and a slope of $S_{MZI} = 70\ mrad.s/\%_{C7}$. This value corresponds to the sensitivity of our detector to heptane.

A criterion on heptane peak properties needs to be defined to compute the detector's limit of detection. We consider a peak to be detectable when it stands out three times from the noise, and is no longer at half height than 1.5 s. Data 3σ-noise, defined as the 3 times the standard deviation of the signal baseline over the 20 seconds preceding injection, was found to be 12 milliradians. In the worst case, a peak meeting this criterion has a FWHM of 1.5 seconds, and a height just equal to the noise. Its area can be approximated by multiplying FWHM by height, and equals to $A_{smallest\_detectable\_peak} = 18\ mrad.s$.

These results allow to compute the theoretical limit of detection of our system, which is the smallest heptane concentration that can be detected, expressed as follows:

$$LOD\ [\%_{C7}] = \frac{A_{smallest\_detectable\_peak}\ [rad.s]}{S_{MZI}\ [\frac{rad.s}{\%_{C7}}]}$$

The theoretical detection limit of our system is therefore: LOD = 0.26 % heptane.

In our experiments, the lowest peak we considered detectable corresponds to solution 11, containing 0.5 % of heptane. This is consistent with our theoretical LOD computation.

We now propose a means to get an order of magnitude of the headspace concentration (in ppm) of a solution at a concentration of 0.22 % heptane. Our reasoning for headspace concentration approximation is based on the hypothesis of linearity of heptane evaporation with its concentration in liquid phase:

$$C_{headspace}[ppm] = 10^6 * \frac{P_{sat}(heptane)}{P_{vial}} * \frac{C_{liq}[\%]}{100}$$

In the case of our setup, with $P_{sat}(heptane) = 4.6kPa$, and $P_{vial} = 100\ kPa$, we obtain a LOD of approximately 120 ppm.

This work is the first study where photonic integrated interferometers are implemented as detectors for gas chromatography. As a first proof of concept, in terms of limit of detection, our system is not as good as other GC analyte detection systems presented in the literature ([24], [26], [27]). Further improvement will consist in lengthening the sensing arm, changing the sensing waveguide's geometry to improve guided light interaction with analytes, or functionalizing the sensing waveguide with porous materials which increase the number of adsorption sites neighboring the sensing waveguides ([37], [38]).

Conclusion

This study demonstrates a miniaturized integrated photonic detector for gas chromatography. We optimized the parameters of the integrated Mach Zehnder interferometers to make them as low-loss as possible at a chosen operation wavelength of $\lambda = 850\ nm$. We developed a low-tech photonic die packaging approach suitable for gas chromatography with a dead volume of only 4 µL and set up a gas fluidics systems for automated sample selection and gas chromatography injection. A real-time processing software was developed to compute the chromatographic signal from the optical acquisition of linear images corresponding to the outputs of the integrated MZIs. We succeeded in obtaining, in less than four minutes, a chromatogram for a solution headspace containing three dilute VOCs in liquid phase, with retention times being repeatable by 1%.

The use of Mach-Zehnder interferometers with coherent detection enables single-wavelength operation, paving the way for fast acquisition of gas chromatograms.

Aknowledgments

The authors would like to thank CEA-Leti for the funding of the PhD project that led to these results. The authors also would like to thank all participants in the SiPhoSens project, in particular Fondation Nanosciences and Aryballe. The authors would like to thank everyone involved in CEA-Leti's clean room for their support in manufacturing the silicon photonic wafers and dies. The authors also would like to thank Nicolas GAIGNEBET, for his precious help in Python coding, and Aurélien LEPOETRE, for helping with the packaging process.

References

[1] X. Gong *et al.*, « Deterioration of plant volatile organic compounds in food: Consequence, mechanism, detection, and control », *Trends in Food Science & Technology*, vol. 131, p. 61-76, janv. 2023, doi: 10.1016/j.tifs.2022.11.022.

[2] Y. Feng, Y. Wang, B. Beykal, M. Qiao, Z. Xiao, et Y. Luo, « A mechanistic review on machine learning-supported detection and analysis of volatile organic compounds for food quality and safety », *Trends in Food Science & Technology*, vol. 143, p. 104297, janv. 2024, doi: 10.1016/j.tifs.2023.104297.

[3] M. Khatib et H. Haick, « Sensors for Volatile Organic Compounds », *ACS Nano*, p. 36, 2022, doi: 10.1021/acsnano.1c10827.

[4] B. R. Kim, « VOC Emissions from Automotive Painting and Their Control: A Review », *Environmental Engineering Research*, vol. 16, n° 1, p. 1-9, mars 2011, Consulté le: 1 février 2024. [En ligne]. Disponible sur: https://www.eeer.org/journal/view.php?number=53

[5] S. Sethi, R. Nanda, et T. Chakraborty, « Clinical Application of Volatile Organic Compound Analysis for Detecting Infectious Diseases », *Clin Microbiol Rev*, vol. 26, n° 3, p. 462-475, juill. 2013, doi: 10.1128/CMR.00020-13.

[6] A. H. Jalal, F. Alam, S. Roychoudhury, Y. Umasankar, N. Pala, et S. Bhansali, « Prospects and Challenges of Volatile Organic Compound Sensors in Human Healthcare », *ACS Sens.*, vol. 3, n° 7, p. 1246-1263, juill. 2018, doi: 10.1021/acssensors.8b00400.

[7] L. Spinelle, M. Gerboles, G. Kok, S. Persijn, et T. Sauerwald, « Review of Portable and Low-Cost Sensors for the Ambient Air Monitoring of Benzene and Other Volatile Organic Compounds », *Sensors*, vol. 17, n° 7, Art. n° 7, juill. 2017, doi: 10.3390/s17071520.

[8] X. Feng, H. Wang, Z. Wang, P. Huang, et J. Kan, « Discrimination and characterization of the volatile organic compounds in eight kinds of huajiao with geographical indication of China using electronic nose, HS-GC-IMS and HS-SPME-GC-MS », *Food Chem*, vol. 375, p. 131671, mai 2022, doi: 10.1016/j.foodchem.2021.131671.

[9] S. C. Terry, J. H. Jerman, et J. B. Angell, « A gas chromatographic air analyzer fabricated on a silicon wafer », *IEEE Transactions on Electron Devices*, vol. 26, n° 12, p. 1880-1886, déc. 1979, doi: 10.1109/T-ED.1979.19791.

[10] C.-J. Lu *et al.*, « First-generation hybrid MEMS gas chromatograph », *Lab Chip*, vol. 5, n° 10, p. 1123-1131, oct. 2005, doi: 10.1039/b508596a.

[11] S. Zampolli *et al.*, « Real-time monitoring of sub-ppb concentrations of aromatic volatiles with a MEMS-enabled miniaturized gas-chromatograph », *Sensors and Actuators B: Chemical*, vol. 141, n° 1, p. 322-328, août 2009, doi: 10.1016/j.snb.2009.06.021.

[12] A. Garg *et al.*, « Zebra GC: A mini gas chromatography system for trace-level determination of hazardous air pollutants », *Sensors and Actuators B: Chemical*, vol. 212, p. 145-154, juin 2015, doi: 10.1016/j.snb.2014.12.136.

[13] B. Bourlon *et al.*, « Revisiting gas sampling and analysis with microtechnology: Feasability of low cost handheld gas chromatographs », in *2016 IEEE SENSORS*, oct. 2016, p. 1-3. doi: 10.1109/icsens.2016.7808672.

[14] Y. Qin et Y. B. Gianchandani, « A fully electronic microfabricated gas chromatograph with complementary capacitive detectors for indoor pollutants », *Microsyst Nanoeng*, vol. 2, p. 15049, 2016, doi: 10.1038/micronano.2015.49.

[15] Q.-Y. Cai et E. T. Zellers, « Dual-Chemiresistor GC Detector Employing Monolayer-Protected Metal Nanocluster Interfaces », *Anal. Chem.*, vol. 74, n° 14, p. 3533-3539, juill. 2002, doi: 10.1021/ac025554u.

[16] Q. Zhong, W. H. Steinecker, et E. T. Zellers, « Characterization of a high-performance portable GC with a chemiresistor array detector », *Analyst*, vol. 134, n° 2, p. 283-293, 2009, doi: 10.1039/B810944C.

[17] L. K. Wright et E. T. Zellers, « A nanoparticle-coated chemiresistor array as a microscale gas chromatograph detector for explosive marker compounds: flow rate and temperature effects », *Analyst*, vol. 138, n° 22, p. 6860, 2013, doi: 10.1039/c3an01136d.

[18] R.-S. Jian, R.-X. Huang, et C.-J. Lu, « A micro GC detector array based on chemiresistors employing various surface functionalized monolayer-protected gold nanoparticles », *Talanta*, vol. 88, p. 160-167, janv. 2012, doi: 10.1016/j.talanta.2011.10.025.

[19] S. Narayanan et M. Agah, « Fabrication and Characterization of a Suspended TCD Integrated With a Gas Separation Column », *Journal of Microelectromechanical Systems*, vol. 22, n° 5, p. 1166-1173, oct. 2013, doi: 10.1109/JMEMS.2013.2255117.

[20] R. A. Iglesias, F. Tsow, R. Wang, E. S. Forzani, et N. Tao, « Hybrid separation and detection device for analysis of benzene, toluene, ethylbenzene, and xylenes in complex samples », *Anal Chem*, vol. 81, n° 21, Art. n° 21, nov. 2009, doi: 10.1021/ac9015769.
[21] O. Martin *et al.*, « Modeling and design of a fully integrated gas analyzer using a µGC and NEMS sensors », *Sensors and Actuators B: Chemical*, vol. 194, p. 220-228, avr. 2014, doi: 10.1016/j.snb.2013.12.075.
[22] A. Venkatasubramanian, V. T. K. Sauer, S. K. Roy, M. Xia, D. S. Wishart, et W. K. Hiebert, « Nano-Optomechanical Systems for Gas Chromatography », *Nano Lett.*, vol. 16, n° 11, p. 6975-6981, nov. 2016, doi: 10.1021/acs.nanolett.6b03066.
[23] S. Zampolli *et al.*, « A MEMS-Enabled Deployable Trace Chemical Sensor Based on Fast Gas-Chromatography and Quartz Enhanced Photoacousic Spectoscopy », *Sensors*, vol. 20, n° 1, Art. n° 1, janv. 2020, doi: 10.3390/s20010120.
[24] K. Reddy, Y. Guo, J. Liu, W. Lee, M. K. K. Oo, et X. Fan, « Rapid, sensitive, and multiplexed on-chip optical sensors for micro-gas chromatography », *Lab Chip*, vol. 12, n° 5, p. 901-905, févr. 2012, doi: 10.1039/C2LC20922E.
[25] J. Liu *et al.*, « Fabry−Pérot Cavity Sensors for Multipoint On-Column Micro Gas Chromatography Detection », *Analytical Chemistry*, vol. 82, n° 11, Art. n° 11, juin 2010, doi: 10.1021/ac902956d.
[26] P. Biswas *et al.*, « A Portable Micro-Gas Chromatography with Integrated Photonic Crystal Slab Sensors on Chip », *Biosensors*, vol. 11, n° 9, p. 326, sept. 2021, doi: 10.3390/bios11090326.
[27] K. Scholten, X. Fan, et E. T. Zellers, « A microfabricated optofluidic ring resonator for sensitive, high-speed detection of volatile organic compounds », *Lab Chip*, vol. 14, n° 19, Art. n° 19, août 2014, doi: 10.1039/c4lc00739e.
[28] S. I. Shopova *et al.*, « On-Column Micro Gas Chromatography Detection with Capillary-Based Optical Ring Resonators », *Anal. Chem.*, vol. 80, n° 6, p. 2232-2238, mars 2008, doi: 10.1021/ac702389x.
[29] Y. Sun *et al.*, « Rapid tandem-column micro-gas chromatography based on optofluidic ring resonators with multi-point on-column detection », *Analyst*, vol. 135, n° 1, p. 165-171, déc. 2009, doi: 10.1039/B917154A.
[30] I. Pavelescu, R. Muller, et V. MoagarPoladian, « Analysis and modeling of a silicon micromachined Mach-Zehnder interferometer for pressure sensing », *J. Micromech. Microeng.*, vol. 7, n° 3, p. 214-217, sept. 1997, doi: 10.1088/0960-1317/7/3/035.
[31] H. Porte, V. Gorel, S. Kiryenko, J. P. Goedgebuer, W. Daniau, et P. Blind, « Imbalanced Mach-Zehnder interferometer integrated in micromachined silicon substrate for pressure sensor », *J. Lightwave Technol.*, vol. 17, n° 2, p. 229-233, févr. 1999, doi: 10.1109/50.744229.
[32] R. G. Heideman, R. P. H. Kooyman, et J. Greve, « Performance of a highly sensitive optical waveguide Mach-Zehnder interferometer immunosensor », *Sensors and Actuators B: Chemical*, vol. 10, n° 3, p. 209-217, févr. 1993, doi: 10.1016/0925-4005(93)87008-D.
[33] B. Drapp *et al.*, « Integrated optical Mach-Zehnder interferometers as simazine immunoprobes », *Sensors and Actuators B: Chemical*, vol. 39, n° 1, Art. n° 1, mars 1997, doi: 10.1016/s0925-4005(97)80218-3.
[34] A. Densmore *et al.*, « Silicon photonic wire biosensor array for multiplexed real-time and label-free molecular detection », *Opt. Lett., OL*, vol. 34, n° 23, p. 3598-3600, déc. 2009, doi: 10.1364/OL.34.003598.
[35] M. S. Murib, D. Martens, et P. Bienstman, « Label-free real-time optical monitoring of DNA hybridization using SiN Mach–Zehnder interferometer-based integrated biosensing platform », *JBO*, vol. 23, n° 12, p. 127002, déc. 2018, doi: 10.1117/1.jbo.23.12.127002.
[36] T. Chalyan *et al.*, « AFM1 Detection in Milk by Fab' Functionalized Si3N4 Asymmetric Mach–Zehnder Interferometric Biosensors », *Toxins*, vol. 11, n° 7, Art. n° 7, juill. 2019, doi: 10.3390/toxins11070409.
[37] X. Ma *et al.*, « On-chip integration of a metal-organic framework nanomaterial on a SiO2 waveguide for sensitive VOC sensing », *Lab Chip*, vol. 21, n° 17, p. 3298-3306, sept. 2021, doi: 10.1039/d1lc00503k.
[38] G. Antonacci, J. Goyvaerts, H. Zhao, B. Baumgartner, B. Lendl, et R. Baets, « Ultra-sensitive refractive index gas sensor with functionalized silicon nitride photonic circuits », *APL Photonics*, vol. 5, n° 8, p. 081301, août 2020, doi: 10.1063/5.0013577.
[39] X. Huang *et al.*, « An in-line Mach-Zehnder Interferometer Using Thin-core Fiber for Ammonia Gas Sensing With High Sensitivity », *Sci Rep*, vol. 7, n° 1, Art. n° 1, avr. 2017, doi: 10.1038/srep44994.
[40] A. L. Siarkowski, L. F. Hernandez, B.-H. V. Borges, et N. I. Morimoto, « Sensing based on Mach-Zehnder interferometer and hydrophobic thin films used on volatile organic compounds detection », *Optical Engineering*, vol. 51, n° 5, 2012, doi: 10.1117/1.oe.51.5.054401.
[41] L. Laplatine *et al.*, « Silicon photonic olfactory sensor based on an array of 64 biofunctionalized Mach-Zehnder interferometers », *Opt. Express, OE*, vol. 30, n° 19, p. 33955-33968, sept. 2022, doi: 10.1364/OE.461858.

[42] C. Herrier *et al.*, « IMAGING A SMELL - from plasmonic-based device to an array of Mach-Zehnder Interferometers », présenté à Proceedings of SPIE - The International Society for Optical Engineering, 2022. doi: 10.1117/12.2622141.
[43] R. J. J. van Gulik, B. M. de Boer, et P. J. Harmsma, « Refractive Index Sensing Using a Three-Port Interferometer and Comparison with Ring Resonators », 2017, doi: 10.1109/jstqe.2016.2601899.
[44] R. Halir, L. Vivien, X. Le Roux, D.-X. Xu, et P. Cheben, « Direct and Sensitive Phase Readout for Integrated Waveguide Sensors », *IEEE Photonics Journal*, vol. 5, n° 4, Art. n° 4, août 2013, doi: 10.1109/jphot.2013.2276747.